

# A study of laser jet soldering process with 55 $\mu\text{m}$ tin balls for head gimbal assembly manufacturing

Shoubin Liu\*, Qingjiang Liao\*\*

\*Harbin Institute of Technology Shenzhen Graduate School, Shenzhen 518055, China, E-mail: mesbliu@hitsz.edu.cn

\*\*Harbin Institute of Technology Shenzhen Graduate School, Shenzhen 518055, China, E-mail: m514077@163.com

**crossref** <http://dx.doi.org/10.5755/j01.mech.22.4.16164>

## 1. Introduction

Hard disks are essential components for mass data storage, cloud storage, and large data exchange in IT industries. The head gimbal assembly (HGA), as shown in Fig. 1, a and b, plays a critical role for constructing a highly reliable and cost-effective hard disk. The HGA is constructed by mounting a head slider to a head suspension by soldering. As shown in Fig. 1, c and Fig. 2, the head suspension is composed of a load beam and a tongue piece, and constructed in a branching structure. The tongue piece, also named as a flexure, is elastically touched to the dimple of the load beam. The head slide is actually mounted on the tongue surface for enabling its pitch and roll movements around the dimple under an air bearing condition [1].

Soldering a head slider to a tongue surface can be achieved by using gold ball bonding (GBB) or solder ball bonding (SBB). Currently, the laser jet solder ball bonding (LJSBB) process has been widely used in HGA manufacturing. In contrast to GBB's high cost, massive deformation of head slider, and presence of static electricity, the LJSBB is a non-contact soldering process that boasts several advantages, such as small size of welding spot, reduced deformation, and minimized presence of static electricity. Overall, LJSBB satisfies the requirements of being a miniaturized and highly precise soldering process.

Developed by Pac Tech in 1998, the LJSBB process has been used in MEMS and micro-device packaging as well as in wafer level bumping [2]. LJSBB is a lead-free soldering process, in which tin alloys with a composition of SnAgCu (96.5, 3, 0.5 wt-%), and a diameter larger than 70  $\mu\text{m}$  are generally used. Recently, Oppert et al. conducted a laser jet soldering experiment using tin balls with diameters of 60, 50, 40, and 30  $\mu\text{m}$ . The experimental results demonstrated that the requirements for flip-chip bonding could still be satisfied even when the diameter of the tin ball had been reduced to 30  $\mu\text{m}$ . However, it should be noted that the qualification ratio of soldering decreased with the decrease of tin ball's diameter [3].

In the manufacturing of HGA products, the dimensions of the head slider in length, width, and height have been reduced from 4.064 mm  $\times$  3.186 mm  $\times$  0.871 mm, to 1.235 mm  $\times$  0.7 mm  $\times$  0.23 mm, and further to 1.235 mm  $\times$  0.7 mm  $\times$  0.18 mm. Furthermore, the number of welding spots has been increased from four to six and then increased to nine, and the diameter of the tin ball used in the LJSBB process has been reduced from 120  $\mu\text{m}$  to 90  $\mu\text{m}$  and further reduced around to 55  $\mu\text{m}$ . Correspondingly, the parameters used in the LJSBB process have to be adjusted according to the tin ball's diameter. The resistance

between the tin ball and the welding tip has inevitably increased due to the smaller diameter of the tin ball. Hence, the  $\text{N}_2$  pressure used in the LJSBB process should be increased, and the laser energy should be reduced. Moreover, the tongue piece is made of a piece of stainless steel with a thickness of about 20  $\mu\text{m}$ . The thin tongue piece and its freedom of gimbal movement around the dimple make the soldering more easy to produce micro-deformation, and it must be at a controllable range.

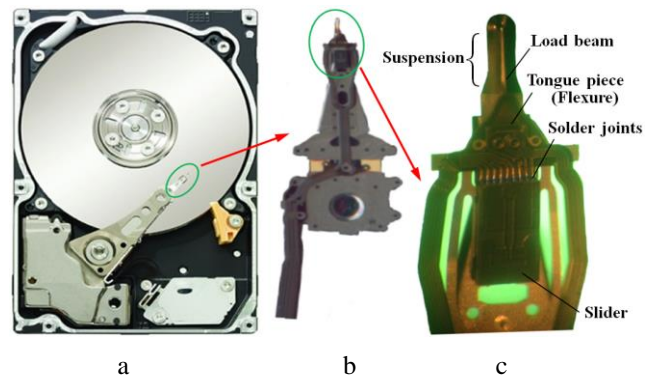


Fig. 1 a - A hard disk; b - HGA; c - and the nine welding spots of the head slider

In this article, the tin ball-based laser jet soldering process used for the manufacturing of nine-welding-spot HGAs was investigated. The tasks of the work are to determine the tin ball's diameter, to find the optimum values of  $\text{N}_2$  pressure and laser energy, and to achieve acceptable micro-deformation of head slider for soldering nine-welding-spot sliders to suspensions with a high qualification ratio. In the following section, the soldering mechanism and the LJSBB procedure were discussed. In addition, the process by which the 55  $\mu\text{m}$  tin ball was accepted for the laser jet soldering of nine-welding-spot HGAs was demonstrated. Then, experiments were conducted on 55  $\mu\text{m}$  tin ball-based laser jet soldering so as to obtain the optimum values of  $\text{N}_2$  pressure and laser energy. Afterwards, the issue of increasing the PSA dispersity of the head slider after soldering was investigated, and measurements were proposed to reduce the micro-deformation level. Finally, several conclusions were revealed.

## 2. LJSBB process and determination of the tin ball's diameter

The HGA LJSBB system used in this study was based on the SB<sup>2</sup>-R-Jet system developed by Pac Tech [2]. This system was coupled with an improved version of laser

system, as shown in Fig. 2. Firstly, the tin ball was transferred from the solder ball feeder to the welding tip, and then, the tin ball was blown to the end of the welding tip under  $N_2$  flow. As the inner diameter of the welding tip was smaller than the diameter of the tin ball, the tin ball got stuck at the end of the tip. However, when the  $N_2$  pressure exceeded the preset value, the laser system emitted a laser pulse that melted the tin ball, and then, the melted tin ball was carried by  $N_2$  flying to the welding position. After wetting and spreading, the solder was cooled immediately and solidified at the welding spot. Moreover, the welding process was achieved under  $N_2$  protection, which prevented oxidation at the welding spot and led to improved wetting force at the welding spot [4, 5].

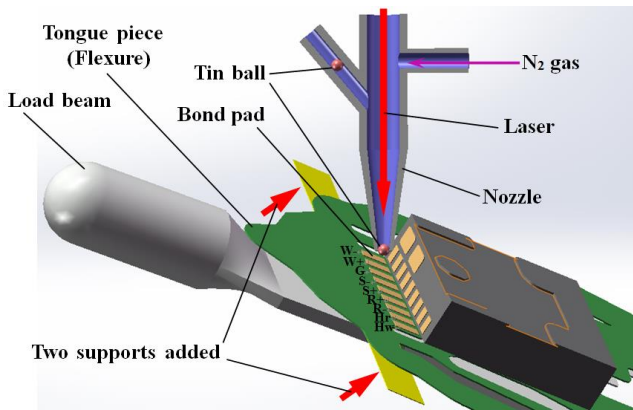


Fig. 2 A schematic illustration of the laser jet soldering process of HGA

The LJSBB process is influenced by several key parameters, two of which are laser energy and  $N_2$  pressure. More specifically, for laser jet solder ball bonding, the laser energy per pulse directly affects the melting of the tin ball and its initial temperature; therefore, the laser energy per pulse is a key parameter in the LJSBB process. From the moment the tin ball was melted until the moment it was blown off the welding tip, a series of mechanics and thermodynamics processes were observed. These processes included the liquid-solid interfacial surface tensions, the van der Waals forces between the melted tin ball and the welding tip, the gravity acting on the tin ball, and finally the heat

dissipation and cooling of the melted tin ball. For micro-objects sized below 1 mm, the adhesion forces between different objects are much greater than their gravity (which is negligible) [6], and these adhesion forces originated from surface tensions, van der Waals forces, and electrostatic forces. With various methods being used to remove static electricity during HGA manufacturing, the jet resistance was primarily a result of surface tensions and van der Waals forces between the solder ball and the welding tip. Therefore, in order to obtain a better welding effect, the  $N_2$  pressure needed to be sufficiently high to overcome the resistance originating from the surface tensions and the van der Waals forces, and to provide a driving force to dispense the tin ball. This relationship thus exemplifies the critical nature of  $N_2$  pressure and solidifies it as another key parameter in the LJSBB process.

For a nine-welding-spot head slider, the features of the vertical soldering pads located at the flank of its end are as follows: the pad size is  $70 \mu\text{m}$  in height and  $60 \mu\text{m}$  in width, the composition of materials is Ta/NiFe/Au (inside to outside), and the thicknesses are  $0.005 \mu\text{m}/0.2 \mu\text{m}/0.8 \mu\text{m}$ . Furthermore, the features of the horizontal soldering pads on the tongue surface are as follows: the pad size is  $80 \mu\text{m}$  in height and  $60 \mu\text{m}$  in width, the composition of materials is Cu/Ni/Au (bottom to top), and the thicknesses are  $8.0 \mu\text{m}/2.0 \mu\text{m}/0.5 \mu\text{m}$ . Soldering the head slider to the tongue surface can be achieved by using tin balls of three diameters: 60, 55 and  $50 \mu\text{m}$ . Material composition of these tin balls is SnAgCu (96.5, 3, 0.5 wt-%). Considering most failures of solder joints were caused by thermal load, a simulation was taken to obtain the stress distributions of welding spots of different tin ball's diameters under the temperature of  $125^\circ\text{C}$  [7, 8]. By using ANSYS software, thermal stresses of nine welding spots were obtained, and only that of the first two spots were shown in Fig. 3. The thermal stresses are caused by the mismatch of the thermal expansion coefficients (TEC) among different materials. The maximum stresses are located at the corner positions of individual spots. It can be found that the distribution of thermal stresses becomes worse as the tin ball's diameter decreased. As shown in Fig. 3, c, the  $50 \mu\text{m}$  tin ball exhibited a worse distribution of thermal stresses among three sets of welding spots.

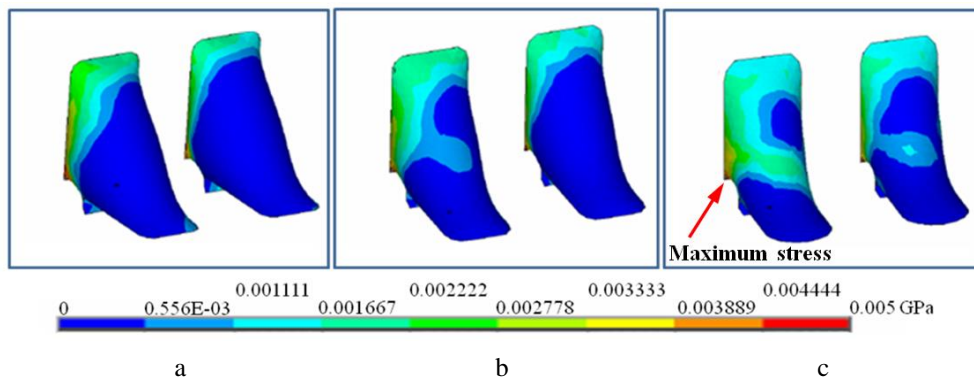


Fig. 3 Simulation of the thermal stresses on the welding spots using tin balls of different diameters: a -  $60 \mu\text{m}$ ; b -  $55 \mu\text{m}$ ; c -  $50 \mu\text{m}$ , under the temperature of  $125^\circ\text{C}$

To verify the simulation results, LJSBB was employed in the manufacturing of HGAs of the same model at a smaller scale. The manufacturing process was repeatedly three times, with each time using a different-sized tin ball of

$60 \mu\text{m}$ ,  $55 \mu\text{m}$ , and  $50 \mu\text{m}$  in diameter in the soldering process. The equipment and parameters adopted, however, remained the same. After this process, three samples were obtained corresponding to the three different-sized tin balls.

Subsequently, a series of reliability tests (including the tensile strength test, mechanical shock test, high temperature and humidity ageing test, and thermal shock test), were conducted on the welding spots of these samples [9, 10]. The thermal shock test was carried out under industrial standards, in which the products were exposed to cycles consisting of 125°C for 0.5 h and then -40°C for 0.5 h [8]. After 300 thermal shock cycles, a scanning electron microscope (SEM) was used to visualize the microstructures of the three samples.

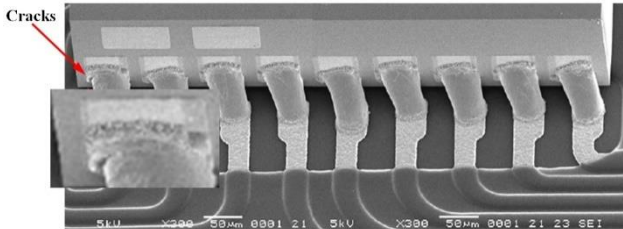


Fig. 4 Fine cracks appeared at the side welding spot using 50  $\mu\text{m}$  tin balls after 300 thermal shock cycles

As illustrated in Fig. 4, it was found that the welding spot using the 50  $\mu\text{m}$  tin ball showed fine cracks, whereas the other welding spots using the 55 and 60  $\mu\text{m}$  tin balls did not exhibit any cracks. The failure of the first welding spot using the 50  $\mu\text{m}$  tin ball could be explained by its worse distribution of thermal stresses causing a stress concentration at its corner. The cyclic thermal stress generated the creep strain, and the creep fatigue failure will further occur at its corner position. The thermal simulation results shown in Fig. 3 correlated well with the experimental results shown in Fig. 4. Based on the simulation and the reliability test results, the tin ball with a small diameter of 55  $\mu\text{m}$  was chosen for the manufacturing of nine-welding-spot HGAs.

### 3. Optimization of parameters of laser jet soldering process

The distribution of laser energy, the value of laser energy, and the  $\text{N}_2$  pressure are three key parameters in LJSBB process. The laser jet soldering based on the 55  $\mu\text{m}$  tin balls has a higher requirement for the distribution of laser energy. In this study, a diode pumped Nd:YAG laser (wavelength = 1064 nm, maximum energy per pulse = 50 mJ, and energy variation within 1%) was used, and the laser pulse can be exported via optical fibers [11]. A laser with a mode structure of  $\text{TEM}_{00}$  can be generated by well tuning the resonant cavity of the laser emitter. A laser beam analyzer (LBA-USB-SP620 by Ophir-Spiricon) verified that the laser energy density followed a Gaussian distribution, as shown in Fig. 5. For the 55  $\mu\text{m}$  tin ball-

based LJSBB, maintaining such initial laser energy distribution is desired.

With the initial laser energy distribution maintained, the optimized values of the laser energy and  $\text{N}_2$  pressure can be obtained via small-batch production by using Design-of-Experiments (DoE) methodology [12]. As a result of a double-factor, three-level full factorial design (FFD), nine experiments were conducted. Additionally, each experiment was repeated, so a total of 18 datasets were obtained as shown in Table 1. The double-factor variance analysis results of the 18 obtained datasets are listed in Table 2.

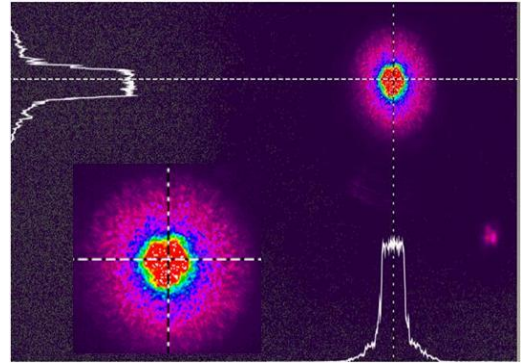


Fig. 5 The energy density of the laser spot followed a Gaussian distribution

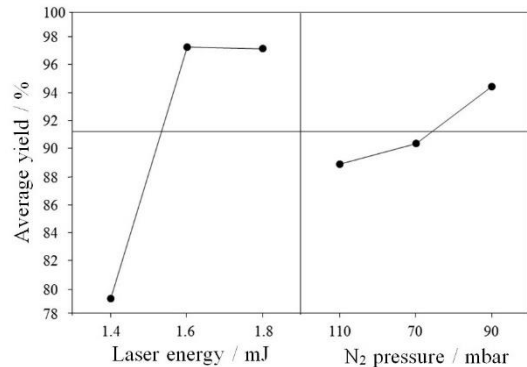


Fig. 6 The main effect plot of the qualification ratio of laser energy and  $\text{N}_2$  pressure

As the interaction was negligible (see Table 2), it could therefore be concluded that the laser energy and  $\text{N}_2$  pressure are the main influencing factors. The average value of the six qualification ratios related to each factor was obtained to form the main effect plot (see Fig. 6). As shown in Fig. 6, the qualification ratio was maximized with laser energy of 1.6 mJ and a  $\text{N}_2$  pressure of 90 mbar. Therefore, 1.6 mJ and 90 mbar were regarded as the optimized values for the laser energy and  $\text{N}_2$  pressure, respectively.

Table 1

Optimization of parameters of the laser jet soldering process based on 55  $\mu\text{m}$  tin balls

Item	1	2	3	4	5	6	7	8	9	10	11	12	13	14	15	16	17	18
Laser energy, mJ	1.8	1.8	1.8	1.6	1.6	1.6	1.4	1.4	1.4	1.8	1.8	1.8	1.6	1.6	1.6	1.4	1.4	1.4
$\text{N}_2$ pressure, mbar	70	90	110	90	110	70	110	70	90	70	90	110	90	110	70	110	70	90
Yield, %	96.5	98.5	96	100	95.5	97.5	73	73.5	88	98.5	97.5	96	99.5	95	96	78	80.5	83

The variance analysis of DoE in the parameter optimization experiments

Item	Degree of freedom (DOF)	Sum of Squares (SS)	Mean of square value (MS)	F-distribution Value	Probability
Laser energy	2	0.127808	0.0639042	107.75	0.000
N <sub>2</sub> pressure	2	0.009700	0.0048500	8.18	0.009
Interaction	4	0.004467	0.0011167	1.88	0.198
Error	9	0.005338	0.0005931		
Total	17	0.147312			

Before large-scale HGA production, the effects of the new parameter values on the key properties of the products were evaluated. The key properties of HGA products include welding spot reliability, pitch static angle (PSA), raw static angle (RSA), A-dim, B-dim, and LG. Initially, a small batch of HGA products was manufactured using the new 55  $\mu\text{m}$  tin ball-based LJSBB. Fig. 7 shows a SEM image of the welding spot cross-section. As can be seen, a homogeneous Au-Sn intermetallic compound (Au-Sn IMC) was observed at the pad/tin ball interface, and no pores were generated on the welded section, thus indicating a good quality of the new soldering process.

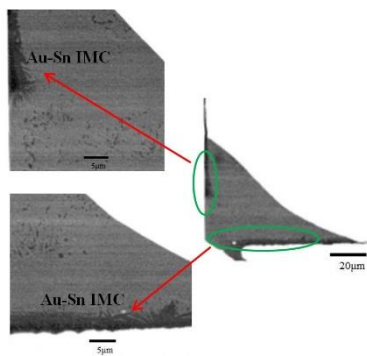


Fig. 7 SEM image of the welding spot cross-section

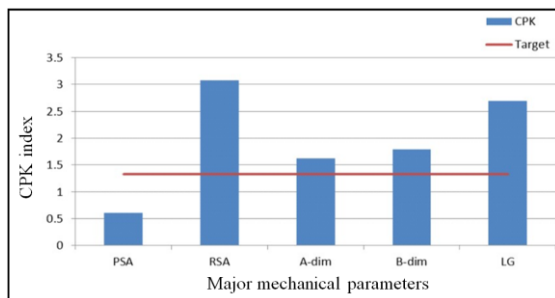


Fig. 8 CPK indices of the five major mechanical parameters of HGA products

Fig. 8 shows the complex process capability (CPK) indices of the five major mechanical properties of HGA products. The industrial standards suggest that a new soldering process in which all CPK indices  $> 1.33$  can be applied to manufacturing. The CPK indices of four of the parameters exceeded the critical level; however, the CPK index of PSA was 0.61. Further investigation revealed that the standard deviation  $\sigma$  of the PSA differential value before and after soldering was around 13, while that corresponding to a CPK of 1.33 was around 7.8. This indicated that the PSA dispersity of the HGA products was increased by the new 55  $\mu\text{m}$  tin ball-based LJSBB.

#### 4. Improvement of soldering micro-deformation

The pitch static angle (definition shown in Fig. 9) is a parameter that is directly related to the flying height of the head slider, thus affecting the read-and-write stability of hard disks. Any variations to the pitch static angle are usually caused by HGA's micro-deformations. In the new 55  $\mu\text{m}$  tin ball-based LJSBB, thermal stresses that resulted from the cooling shrinkage of the welding spot initiated a drag force, and this force may lead to a micro-deformation, thereby resulting in increased PSA dispersity of HGA products.

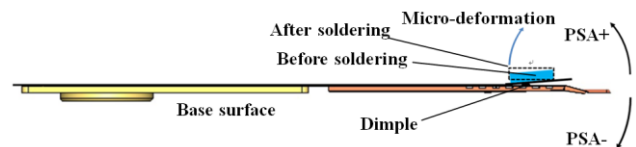


Fig. 9 A schematic illustration of the PSA and the micro-deformation of HGA products

With the soldering sequence altered, the micro-deformation of the welding spot, as well as its impact on PSA could be decreased due to mutual suppression between different deformations. Therefore, optimizing the soldering sequence may alleviate the issue of increasing PSA dispersity. Moreover, the optimization of the soldering sequence should be based on several constraints such as minimizing soldering shift, prioritizing the ESD ground pad, and posterior welding two read pads. As shown in Fig. 2, the initial sequence was W-, W+, G, S-, S+, R+, R-, Hr, Hw; however, to counteract thermal stresses, symmetric soldering was used from the outside-in, and the sequence was changed to Hw, W-, W+, G, S-, S+, R+, R-, Hr. Keeping the other soldering parameters constant, a small batch of HGA products was manufactured. The standard deviation of the PSA differential value of the new batch decreased to 8, and an F-test confirmed this significant improvement. However, the CPK index of PSA of the new batch was 1.07 (critical value is 1.33), and further improvement is required.

Additional mechanical supports to the tongue piece were also designed so as to counteract thermal stresses. The concentrated stress in the welding spot led to a slight deformation of the tongue piece in that area. In order to prevent the micro-deformation, additional mechanical supports were incorporated in order to relieve stress on the tongue piece, which can reduce the impact of the new process on the PSA value. In this study, two additional mechanical supports were placed near the outriggers of tongue piece, as shown in Fig. 2. A new fixture with the mechanical supporting part was manufactured for HGA volume production.

With the soldering sequence modified and additional supports added, another small batch of HGA products was manufactured using the proposed soldering process. The products exhibited a standard deviation of 6.3 (previously 10.9), and an average differential value of 1.2 (previously -18.9). The F-test confirmed this significant improvement, and moreover, the products manufactured in this way showed a CPK index higher than 1.33. Other experiments verified that the additional supports did not significantly affect the other parameters of the HGA products. Therefore, it is reasonable to conclude that the previous negative effects of the new 55  $\mu\text{m}$  tin ball-based laser jet soldering process on the PSA values were eliminated. Over 2,000 pieces of HGA products were manufactured by the modified soldering process, i.e. additional supports involved, modified soldering sequence, laser energy density with Gaussian distribution, 1.6 mJ laser energy, and 90 mbar  $\text{N}_2$  pressure. The resulting qualification ratio is approximately 99.3%.

## 5. Conclusions

In this article, we proposed a new laser jet soldering process based on 55  $\mu\text{m}$  tin balls for the manufacturing of nine-welding-spot HGAs. Firstly, it was found that the jet resistance was increased as the diameter of the tin ball decreased. The  $\text{N}_2$  pressure should be sufficiently high so as to overcome these resistive forces caused by the surface tensions and van der Waals forces between the melted tin ball and the welding tip. Laser energy should be reduced as the diameter of tin ball decreased. Then, optimization experiments for sifting process parameters were carried out and it was determined that the optimized laser energy and the  $\text{N}_2$  pressure were 1.6 mJ and 90 mbar, respectively. In addition, the increasing of PSA dispersity of HGA products can be counteracted by modifying the soldering sequence and incorporating two additional supports on the tongue piece. Finally, volume production of HGA showed that the proposed laser jet soldering process based on 55  $\mu\text{m}$  tin balls can manufacture HGA products with a qualification ratio of approximately 99.3%.

## References

1. **Tang, Z.** 2013. Touch-down induced contact and friction forces at the dimple/gimbal interface, *Microsyst. Technol* 19: 1625-1632. <http://dx.doi.org/10.1007/s00542-013-1872-2>.
2. **Kasulke, P.; Schmidt, W.; Titerle, L.; Bohnaker, H.** 1998. Solder ball bumper SB<sup>2</sup>—a flexible manufacturing tool for 3-dimensional sensor and microsystem packages, *IEEE/CPMT International Electronics Manufacturing Technology Symposium* 70-75. <http://dx.doi.org/10.1109/IEMTE.1998.723062>.
3. **Oppert, T.; Teutsch, T.; Azdasht, G.; Zakel, E.** 2012. Micro ball bumping packaging for wafer level & 3-D solder sphere transfer and solder jetting, *IEEE/CPMT International Electronics Manufacturing Technology Symposium*, 1-6. <http://dx.doi.org/10.1109/IEMT.2012.6521835>.
4. **Baated, A.; Jiang, J.; Kim, K.S.** 2010. Sn-Ag-Cu soldering reliability as influenced by process atmosphere, *IEEE Transactions on Electronics Packaging Manufacturing* 33(1): 38-43.

- <http://dx.doi.org/10.1109/TEPM.2009.2035442>.
5. **Stratton, P.** 2005. Nitrogen's effect on Pb-free soldering, *Circuits Assembly* 16(2): 50-51.
6. **Fearing, R.** 1995. Survey of sticking effects for micro parts handling, *IEEE/RSJ Int. Conf. on Intell. Robot. Syst.* 2: 212-217. <http://dx.doi.org/10.1109/IROS.1995.526162>.
7. **Tong, Y.T.; Zhong, Z.** 2004. Board level solder joint reliability analysis and optimization of pyramidal stacked die BGA packages, *Microelectronics Reliability* 44(12): 1957-1965. <http://dx.doi.org/10.1016/j.microrel.2004.04.019>.
8. **Chen, H.; Wang, C.; Li, M.** 2006. Numerical and experimental analysis of the Sn3.5Ag0.75Cu solder joint reliability under thermal cycling, *Microelectronics Reliability* 46(8): 1348-1356. <http://dx.doi.org/10.1016/j.microrel.2005.12.001>.
9. **Zeng, K.; Tu, K.** 2002. Six cases of reliability study of Pb-free solder joints in electronic packaging technology, *Materials Science and Engineering R Reports* 38(2): 55-105. [http://dx.doi.org/10.1016/S0927-796X\(02\)00007-4](http://dx.doi.org/10.1016/S0927-796X(02)00007-4).
10. **Bieler, T. et al.** 2008. Influence of Sn grain size and orientation on the thermomechanical response and reliability of Pb-free solder joints, *IEEE Transactions Components and Packaging Technologies* 31(2): 370-381. <http://dx.doi.org/10.1109/TCAPT.2008.916835>.
11. **Steen, W.** 2010. *Laser material processing*, Springer Science & Business Media, 199-249. <http://dx.doi.org/10.1179/1743280411Y.0000000003>.
12. **Montgomery, D.** 2005. *Design and Analysis of Experiments*, 6th edition, New York: Wiley, 643 p.

Shoubin Liu, Qingjiang Liao

A STUDY OF LASER JET SOLDERING PROCESS WITH 55  $\mu\text{m}$  TIN BALLS FOR HEAD GIMBAL ASSEMBLY MANUFACTURING

## S u m m a r y

This paper presented a study of the laser jet soldering process based on 55  $\mu\text{m}$  tin balls. In the tin ball-based laser jet soldering, the  $\text{N}_2$  pressure should be increased and the laser energy value should be decreased as the diameter of the tin ball decreased. Moreover, the distribution of laser energy significantly affected soldering quality. Through using DoE methodology, the optimized parameters for laser jet soldering based on 55  $\mu\text{m}$  tin balls were obtained. To eliminate the increasing of dispersity of the pitch static angle (PSA) caused by soldering micro-deformation, an optimized soldering sequence and two additional supports on tongue piece were taken. Volume production showed that the proposed laser jet soldering process based on 55  $\mu\text{m}$  tin balls can manufacture HGA products with a qualification ratio of approximately 99.3%.

**Keywords:** laser jet solder ball bonding, soldering process, head gimbal assembly, head slider, tin balls.

Received November 06, 2015  
Accepted July 04, 2016